Novel merwinite/akermanite ceramics*: in vitro* bioactivity

I. K. Mihailova[1,*], L. Radev[1], V. A. Aleksandrova[1], I. V. Colova[1], I. M. M. Salvado[2], M. H. V. Fernandes[2]

[1] *University of Chemical Technology and Metallurgy, 8 St. Kl. Ohridski Blvd., Sofia 1756, Bulgaria*

[2] *University of Aveiro and CICECO, Aveiro, Portugal*

* E-mail : irena@uctm.edu

Abstract

The ceramics in the system CaO – MgO – SiO_2 has recently received a great deal of attention because they exhibit good *in vitro* bioactivity and have potential use as bone implants. Biphasic calcium-magnesium-silicate ceramics was prepared by a sol-gel method. The dried gel with chemical composition $3CaO.MgO.2SiO_2$ was thermally treated at 1300°C for 2 h. The structural behavior of the synthesized ceramics was examined by means of X-ray diffraction (XRD), Fourier Transform Infrared Spectroscopy (FTIR) and Scanning Electron Microscopy (SEM). Merwinite, as the main crystalline phase, and akermanite, as the minor phase, were identified. The *in vitro* bioactivity of the synthesized ceramic samples was recorded in Simulated Body Fluid (SBF) for different times of soaking. The apatite formation on the surface of the immersed samples was detected by FTIR, SEM and Energy Dispersive Spectroscopy (EDS) techniques. The ion concentrations in the SBF solutions after the *in vitro* test were evaluated by Inductively Coupled Plasma Optical Emission Spectrometry (ICP-OES).

On the basis of the results obtained, the ability of the biphasic ceramics to deposit apatite layer was found. The peculiarities of the formation of apatite layer depending on the phase composition were analyzed and discussed.

Key words: CaO – MgO – SiO_2, ceramics, merwinite, akermanite, *in vitro* bioactivity

Introduction

It is quite natural important societal issues and topics related to health and quality of life to attract serious scientific interest. Thus, intensive research has been conducted in recent decades to produce new biomaterials for various applications.

Biomaterials can be classified as bioinert, bioactive and bioresorbable, based on their chemical surface reactivity. Bioactive glasses and ceramics are considered as potential materials for bone substitutes, because they can form a direct bond with the living bone. Important requirement for bioactive material is that in the presence of biological fluids, an apatite layer is produced on their surfaces, which provides the bonding interface with living hard tissues [1].

Mg-containing silicate ceramics, glass-ceramics and glasses have proven to be bioactive and exhibit numerous advantages for biomedical applications [2, 3]. Their mechanical properties, bioactivity and biocompatibility make them promising candidates for bone tissue regeneration which explains the growing interest in these materials [3, 4]. The effects of MgO contents on the structure, crystallization, degradability and bioactivity of glasses [5], glass-ceramics [6] and ceramics [7] in the $MgO – CaO – SiO_2 – P_2O_5$ system were investigated. Some authors reported that the crystallization of the glasses decreased their apatite-formation ability [8]. Various studies have investigated ceramics and glass-ceramics in the $CaO – MgO – SiO_2$ system for biomedical applications, including merwinite [4, 9–13], akermanite [14–16], diopside [1, 17, 18] and monticellite [19, 20] ceramics and glass-ceramics. Diba *et al.* [3] summarize and discusse the most relevant studies carried out in the field of Mg-containing bioactive silicate ceramics and glass-ceramics.

Research carried out so far on materials containing merwinite as the main phase reveals their promising properties for use as biomaterials [4, 9–13, 21]. The properties of three single-phase (merwinite, akermanite, and monticellite) ceramics with different MgO contents were compared and the relationship between the chemical composition and the mechanical and biological properties was investigated [20]. The results obtained by Chen *et al.* [21] showed that the mechanical properties of bioceramics in the $MgO – CaO – SiO_2$ system were improved from merwinite to akermanite and monticellite ceramics with the increase of MgO contents, whereas the apatite-formation ability in SBF and cell proliferation decreased. Their results indicated that the MgO content was one of the important factors, which distinctly affected the mechanical properties and biological performances of bioceramics.

Despite the positive results of merwinite ceramics bioactivity, the publications related to this phase are much less than the ones dedicated to other calcium magnesium silicates as diopside, akermanite and more [3]. Furthermore, in a series of publications dedicated to nanocrystalline merwinite, the phase is synthesized using the sol-gel molar ratio of $TEOS:Mg(NO_3)_2.6H_2O:Ca(NO_3)_2.4H_2O$ =

1:1.44:0.85 [1, 8–13]. This composition of the gel is significantly different from the stoichiometry of merwinite and the obtained and tested materials are obviously quite a specific case of merwinite bioceramics. In the present study, the composition of the initial gel was selected corresponding to the stoichiometry of merwinite $3CaO.MgO.2SiO_2$ to synthesize ceramics, wherein merwinite is prevalent and to examine its structure and bioactive properties.

Experimental

Sample preparation

Ceramics was prepared by sol-gel method using tetraethyl orthosilicate ($(C_2H_5O)_4Si$, TEOS), magnesium nitrate hexahydrate ($Mg(NO_3)_2.6H_2O$) and calcium nitrate tetrahydrate ($Ca(NO_3)_2.4H_2O$) as raw materials. Nitric acid (HNO_3, 2 N) was used to catalyze the hydrolysis of TEOS. The TEOS was mixed with absolute ethanol, water and 2N HNO_3 (molar ratio: $TEOS/H_2O/HNO_3$=1:8:0.16) and hydrolyzed for 1 h. under stirring. Then, the solutions of $Ca(NO_3)_2.4H_2O$ and $Mg_2(NO_3).6H_2O$ were added into the mixture (molar ratio: $TEOS/Mg(NO_3)_2.6H_2O/Ca(NO_3)_2.4H_2O$ = 2:1:3), and reactants were stirred for 6 h at room temperature. After mixing, the solution was dried at 100 °C for 2 days to obtain the dry gel. The dried gel was calcined at 700 °C for 2 h. Finally, the powders were thermally treated at 1300 °C for 2 h.

Characterization techniques

X-ray powder diffraction (XRD) analysis was applied for phase identification. An X-ray diffractometer Philips at Cu Kα radiation was used in the range from 8° to 90° 2θ (step size: 0.05°, counting time per step: 1 s). The crystalline phases were identified using the powder diffraction files JCPDS: 35-0591 and JCPDS: 35-0592 from database JCPDS – International Centre for Diffraction Data PCPDFWIN v.2.2. (2001). The quantitative phase analysis and the determination of unit cell parameters of crystalline phases was performed with the PowderCell 2.4 software [22]. FTIR spectroscopy was applied. Infrared transmittance spectra were recorded by using the pressed-pellet technique in KBr. KBr pellets were prepared by mixing of ~1 mg of the sample with 300 mg KBr. The measurements were made with a FTIR spectrometer Brucker Tensor 27 in the frequency range from 4000 to 400 cm^{-1}. The transmittance spectra were recordered using MCT detector with 64 scans and 1 cm^{-1} resolution.

The morphology of the surface and chemical composition were analyzed using Scanning Electron Microscopy SEM Hitachi SU–70 equipped with energy dispersive spectrometer (EDS).

SBF *in vitro* test

In order to estimate the *in vitro* bioactivity (potential of apatite formation) of the sample, we used the Simulated Body Fluid (SBF) proposed by Kokubo et al. [23], the Tris-buffered SBF (Na^+ 142.0, K^+ 5.0, Mg^{2+} 1.5, Ca^{2+} 2.5, Cl^- 147.8, HCO_3^- 4.2, HPO_4^{2-} 1.0 and SO_4^{2-} 0.5 mol m^{-3}; 7.4 pH). The concentration of various ions in the SBF was adjusted to be similar to those in human blood plasma.

0.3 g of the homogenized ceramic powders were uniaxially pressed to obtain pellets 2 mm in thickness and 10 mm in diameter. The pellets were placed in polyethylene bottles containing 20 ml of SBF at 37 ± 0.5 °C. The sample surface area to SBF volume (SA/V) ratio was equal to 0.1 cm^{-1}.

Pellets were removed after 7 and 14 days of soaking, gently rinsed with deionized water and acetone, and dried at room temperature.

Sample surfaces and cross-sections, before and after SBF treatment, were examined by SEM and EDS. The changes in the samples during the *in vitro* test were also registered by FTIR spectroscopy.

The SBF was removed after several periods of immersion and calcium, magnesium, phosphorus, and silicon ion concentration in the removed SBF was determined by inductively coupled plasma optical emission spectrometry (Prodigy High Dispersion ICP-OES Spectrometer from Teledyne Leeman Labs – USA).

Results and discussion

- ***Phase composition and microstructure of ceramic***

XRD data corresponding to the synthesized sample are shown in Fig. 1. Merwinite $Ca_3MgSi_2O_8$ (JCPDS: 35-0591), as the main crystalline phase, and akermanite $Ca_2MgSi_2O_7$ (JCPDS: 35-0592), as the minor phase, were identified in ceramic sample sintered at 1300 °C for 2 h. The phase composition and lattice parameters for crystalline phases are presented in Table 1. The quantitative phase analysis and calculation of the lattice parameters were performed with the PowderCell 2.4 software. The values of lattice parameters observed for merwinite and akermanite in the ceramic were very close to those of the standard JCPDS and thus no difference in their crystal structures was detected.

As it can be seen, on Fig. 2, the presented FTIR spectrum corresponds to the spectrum of merwinite [24, 25]. The intensive bands posited in the range 850-1050 cm^{-1} correspond to internal antisymmetric and symmetric stretching vibrations of SiO_4 tetrahedra in merwinite [25]. In the same range the most intensive band, posited at 936 cm^{-1} is related to the non-bridging oxygen (NBO) bonds of Si-O-Ca [26]. The other intensive bands in the region 450 to 550 cm^{-1} could be assigned to Si-O-Si bending vibration [25]. In the FTIR spectrum of the thermally treated sample (Fig. 2), the peaks near 1022, 936, 885, 530 and 515 cm^{-1} confirm merwinite as a dominant phase, while the peaks near 975, 905, 681, 635 and 472 cm^{-1} as well as low frequency shoulder around 850 cm^{-1} could be related to akermanite [24–28]. Both phases reveal a peaks near 936 and 587 cm^{-1}. The presented FTIR results are in good agreement with XRD analysis.

SEM images of the thermally treated ceramic sample before *in vitro* test are given in Fig. 3. From the depicted SEM images of the sample before immersion in SBF it was observed that the surface was well crystallized. The euhedral crystals do not exeed 3 μm (Fig. 3 b).

- ***In vitro* bioactivity of merwinite-akermanite ceramic**

FTIR spectra of the ceramic samples after soaking in SBF solution for 7 and 14 days in static conditions are presented at Fig. 4. Four vibrational modes are visible for the PO_4^{3-} ions in apatite: $\nu_1PO_4^{3-}$ at 960-966 cm^{-1}, $\nu_2PO_4^{3-}$ at 460 cm^{-1}, $\nu_3PO_4^{3-}$ at 1190-980 cm^{-1}, and $\nu_4PO_4^{3-}$ at 660-520 cm^{-1} [29, 30]. The most intensive peak in the infrared spectra should be the peak arising from antisymmetric stretching ν_3 of phosphate group. After SBF soaking a gradual change in the intensity ratio of the peaks in the spectral range 850-1050 cm^{-1} occurred which could be an indication for increased amount of apatite on the surface.

In our FTIR results, presented in Fig. 4 some new peaks can be observed. These new peaks were posited at 452 (453) $cm^{-1,}$ and 472 (471) cm^{-1}. They could be ascribed to $\nu_2PO_4^{3-}$ [31, 32]. The additional peaks at 619 (620) cm^{-1} and 667 cm^{-1} (for the two samples) were assigned to $\nu_4PO_4^{3-}$ [33, 34]. On the other hand, the peak centered at 667 cm^{-1} could be related also to OH^- [35]. The peak at 903 (906) cm^{-1} was characteristic of $\nu_1PO_4^{3-}$ [36]. In FTIR spectra for the sample after soaking for 7 days (Fig. 4, a) one additional peak at 996 was visible, which could be assigned to $\nu_1PO_4^{3-}$ [37].

Furthermore, in the presented FTIR spectra we were able to observe the presence of a series of peaks, centered at 718 cm^{-1}, 744 cm^{-1}, and 856 (855) cm^{-1}, which were assigned to $\nu_4CO_3^{2-}$ and $\nu_2CO_3^{2-}$ vibrational modes[38, 39].

From the presented infrared results we could assume that the presence of ν_1-ν_4 PO_4^{3-} could be related to the crystalline calcium phosphates formed on the surface of the immersed samples. Moreover, $CaCO_3$ was also formed on the soaked samples.

In addition, on the basis of the depicted results four types of regions of $\nu_3CO_3^{2-}$ could be detected: 1410-1430 cm^{-1}, 1430-1460 cm^{-1}, 1460-1500 cm^{-1}, and 1500-1560 cm^{-1}. In the case of our samples, the peaks' position can be related as follows:

- For B-type carbonate-containing apatites in which CO_3^{2-} replaced PO_4^{3-} at 1416 cm^{-1} [40], 1420 cm^{-1} [41], 1438 (1433) cm^{-1} [42], 1455 cm^{-1} [43], 1471 (1476) cm^{-1} [41], 1486 cm^{-1} [44], and 1490 cm^{-1} [44]. We must note that the peaks at 1420 and 1490 cm^{-1} could be also related to vaterite [39]. The peak centered at 1476 cm^{-1} was assigned to aragonite, and the one at 1438 cm^{-1} to calcite [39].
- For A-type carbonate-containing apatites in which CO_3^{2-} replaced OH^- at 1504 cm^{-1} [31], 1517 (1519) cm^{-1} [45], 1533 (1536) cm^{-1} [46], and 1552 (1556) cm^{-1} was found.

On the basis of the results related to the presence of CO_3^{2-} bands we can conclude that B-type and A-type carbonate-containing apatites were formed on the immersed ceramics. B-type was a predominant type for carbonate-containing apatites on the ceramics after in vitro test in SBF for 7 and 14 days in static conditions.

SEM micrographs of the ceramic sample, after immersion in SBF for 7 and 14 days in static conditions are presented in Fig. 5. After 7 days of immersion in SBF the surface was fully covered by the multiple sphere-like particles (typical size 0.5 - 1 μm) due to the interaction of the ceramic surface with the SBF solution (Fig. 5 a, b). The surface of the sample after a longer test period (14 days) was completely covered by spherical aggregates. On the micrograph (Fig. 5 d) the crystals that make up the spherical shapes are easier to distinguish. This type of morphology is typical of carbonate-containing apatites formations.

The detected changes on the sample surface and the identification of the morphology typical of the apatite crystalline aggregates made it necessary to conduct an EDS analysis and the obtained data is shown in Fig. 6. In this context, EDS analysis proved the presence of large amount of Ca (15.05 at. %) and P (7.43 at. %). The quantity of Si was 2.92 at. %. Moreover, EDS revealed the presence of small amount of Mg (0.91 at. %). On the basis of the results obtained (Ca+Mg)/(Si+P)=1.54. This ratio was less than the stoichiometric value of 1.67 for pure apatite, i. e. calcium deficient apatite was formed on the surface of the immersed ceramics.

On the other hand, after soaking for 14 days (Fig. 6, b), EDS proved the presence of Ca (21.58 at. %), P (11.22 at. %), Si (2.09 at. %), and Mg (0.60 at. %), i. e. (Ca+Mg)/(Si+P)=1.67. As it can be seen, apatite layer was formed on the surface of the immersed glass-ceramics after 14 days of soaking.

On the basis of the results obtained we can suppose that two types of substitutions can be produced: (i) $Mg^{2+} \rightarrow Ca^{2+}$ and/or (ii) $CO_3^{2-} \rightarrow PO_4^{3-}$ and $SiO_4^{4-} \rightarrow PO_4^{3-}$ [34].

The release profiles of Si, Ca, Mg and P ions in SBF at 37 °C for ceramic samples are shown on Fig. 7. The ceramic material released Ca and Si ions, and removed P ions from SBF. The concentration of Ca in SBF increased from 116 (for SBF solution) to 952 mg/l for ceramics, when soaked at 37 ± 0.5 °C for 14 days. The continuous Ca^{2+} ion dissolution of the ceramics contributed to generate an increase in the Ca^{2+} ion concentration in the SBF despite the formation of apatite phase. During the first and second week, the concentration of Ca in SBF increased rapidly and evenly. After 7 days phosphorous ions were fully removed from SBF by the ceramics, because of the formation of apatite phase on the surfaces. In addition, SBF was enriched in Si^{4+} up to a value of 57 mg/l for 7 days. After 14 days, a relatively lower concentration of Si was detected.

After 7 days of soaking, the concentration of Mg in SBF increased slightly from 42 to 53 mg/l but after 14 days the concentration decreased and Mg^{2+} ions were removed from SBF by the ceramics. On the one hand, the obtained results suggested low partial dissolution of Mg^{2+} and Si^{4+} ions of merwinite-akermanite ceramics, on the other hand, the decrease in their concentration during the second week of immersion may be due to the their inclusion in the formation of the surface apatite layer.

After 7 days of soaking a depletion of P ion concentration from the SFB solution was found. However, this did not delay the apatite-like formation process. The obtained SEM and EDS data indicated that the crystallization and growth of the apatite layer continued. Furthermore, with the increase of soaking time, the release of Ca^{2+} led to supersaturation of the Ca ions in the solution and aided the formation of apatite like layer.

The release profile of Ca was similar to the data published by Radev [34] for $CaO - SiO_2 - P_2O_5$ glass-ceramics containing β-Ca_2SiO_4 and $Ca_{15}(PO_4)_2(SiO_4)_6$. The microstructural characteristics of the surface after 14 days in SBF were also similar.

In accordance with Diba *et al.* [3] the bioactivity mechanism of the Mg-containing silicate ceramics is similar to those suggested for Mg-containing bioactive silicate glasses. Studies have

shown a relationship between the degradation rate and bioactivity of the ceramics in the CaO – MgO – SiO_2 system [21]. The key role of degradation in the bioactivity process of these materials is correlated to the ion exchange rate of the ceramics/media interface which affects the formation of a silica-rich layer on the ceramic surface [1, 3, 47]. The silanol groups formed on the surface induce heterogeneous nucleation of apatite, and the released calcium ions increase the ionic activity product of apatite, enhancing apatite nucleation. The dissolution behavior of merwinite-akermanite ceramics was generally in accordance with the previously established apatite-forming mechanism. Therefore, the mechanism of apatite formation on the merwinite-akermanite ceramics might be similar to that of the CaO – SiO_2 – MgO based bioactive ceramics.

Conclusion

In conclusion, biphasic merwinite-akermanite bioceramics in the MgO – CaO – SiO_2 system was prepared first, and then their structural properties and *in vitro* bioactivity were evaluated. After 7 days of immersion of the ceramic samples in SBF, sphere-like Ca-P particles were formed on the surface and continued to grow during the 14 days of immersion. The results indicated that the merwinite-akermanite ceramics had high reactivity in SBF, ability to form an apatite-like layer and potentially it might be used as bioactive implant material. The dissolution behavior of ceramics was generally in accordance with the previously established apatite-forming mechanism on the surface of CaO–SiO_2–MgO based bioactive ceramics in SBF.

Acknowledgements

This work was funded by University of Chemical Technology and Metallurgy – Sofia, Bulgaria through research projects № 11308 and № 11167.

Нова мервинит/акерманитова керамика*: in vitro* биоактивност

И. К. Михайлова[1,*], Л. Радев[1], В. А. Александрова[1], И. В. Цолова[1], И. М. М. Салвадо[2], М. Х. В. Фернандес[2]

[1] *Химикотехнологичен и металургичен университет, бул. „Св. Климент Охридски“ № 8, София, 1756, България*

[2] *Авейро Университет и CICECO, Авейро, Португалия*

Резюме

Керамиката в системата CaO – MgO – SiO_2 напоследък е обект на засилен интерес, защото проявява добра *in vitro* биоактивност и може да се използва за костни импланти. Двуфазна калциево-магнезиево-силикатна керамика е получена по зол-гелен метод. Сухият гел с химичен състав $3CaO.MgO.2SiO_2$ е термично третиран при 1300°C за 2 ч. Структурата на синтезираната керамика е изследвана с рентгенофазов анализ, инфрачервена спектроскопия с Фурие трансформация (ИЧ) и сканираща електронна микроскопия (СЕМ). Установени са мервинит, като основна фаза и акерманит – като съпътстваща. Биоактивността *in vitro* на синтезираните керамични образци е определена в симулирана телесна течност (SBF) за различно време на потапяне. Образуването на апатит на повърхността на потапяните образци е регистрирано с ИЧ, СЕМ и енергийно дисперсивна спектроскопия. Промените в концентрацията на йони в SBF след *in vitro* тестовете е определена с оптична емисионна спектроскопия с индуктивно свързана плазма.

На база на получените резултати добра *in vitro* биоактивност е установена за двуфазната керамика. Анализирани и дискутирани са особеностите на образуване на апатитов слой в зависимост от фазовия състав на керамиката.

References

1. M. A. Sainz, P. Pena, S. Serena, A. Caballero, *Acta Biomaterialia*, **6**, 2797 (2010).
2. M. Diba, F. Tapia, A. R. Boccaccini, L.A. Strobel, *Int. J. Appl. Glass. Sci.*, **3**, 221 (2012).
3. M. Diba, O.-M. Goudouri, F. Tapia, A. R. Boccaccini, *Current Opinion in Solid State and Mater. Sci.*, **18**, 147 (2014).
4. A. Nadernezhad, F. Moztarzadeh, M. Hafezi, H. Barzegar-Bafrooei, *J. Eur. Ceram. Soc*, **34**, 4001 (2014).
5. J. Ma, C. Z. Chen, D. G. Wang, Y. Jiao, J. Z. Shi, *Colloids and Surfaces B: Biointerfaces*, **81**, 87 (2010).
6. J. Ma, C. Z. Chen, D. G. Wang, X. Shao, C. Z. Wang, H. M. Zhang *Ceram. Int*., **38**, 6677 (2012).
7. J. Ma, C. Z. Chen, D. G. Wang, J. H. Hu, *Materials Letters*, **65**, 130 (2011).
8. J. Ma, C. Z. Chen, D. G. Wang, J. H. Hu, *Ceram. Int.*, **37** 1637 (2011).
9. J. Ou, Y. Kang, Z. Huang, X. Chen, J. Wu, R. Xiao, G. Yin, *Biomed. Mater.*, **3**, 015015 (2008).
10. M. Hafezi-Ardakani, F. Moztarzadeh, M. Rabiee, A. R. Talebi, M. Abasi-shahni, F. Fesahat and F. Sadeghian, *J. Ceram. Process. Res.*, **11**, 765 (2010).
11. M. Hafezi-Ardakani, F. Moztarzadeh, M. Rabiee, A. R. Talebi, *Ceram. Int.*, **37**, 175 (2011).
12. M. Hafezi, A. R. Talebi, S. M. Miresmaeili, F. Sadeghian, F. Fesahat, *Ceram. Int.*, **39**, 4575 (2013).
13. M. Razavi, M. Fathi, O. Savabi, B. H. Beni, D. Vashaee, L. Tayebi, *Ceram. Int.*, **40**, 9473 (2014).
14. R. K. Singh, A. Srinivasan, *Ceram. Int*., **36**, 283 (2010).
15. M. Razavi, M. Fathi O. Savabi, S. M. Razavi, B. H. Beni, D. Vashaee, L.Tayebi, *Ceram. Int*., **40**, 3865 (2014).
16. X. Hou, G. Yin, X. Chen, X. Liao, Y. Yao, Z. Huang, *Appl. Surf. Sci.*, **257**, 3417 (2011).
17. C. Wu, Y. Ramaswamy, H. Zreiqat, *Acta Biomaterialia*, **6**, 2237 (2010).
18. C. P. Yoganand, V. Selvarajan, L. Lusvarghi, O. M. Goudouri, K. M. Paraskevopoulos, M. Rouabhia, *Mater. Sci. Eng. C*, **29**, 1759 (2009).
19. S. Ni, L. Chou, J. Chang, *Ceram. Int.*, **33**, 83 (2007).
20. S. Ni, J. Chang, L. Chou, *J. Mater. Sci.: Mater. Med.*, **19**, 359 (2008).
21. X. Chen, J. Ou, Y. Wei, Z. Huang, Y. Kang, G. Yin, *J. Mater. Sci.: Mater. Med.*, **21**, 1463 (2010).
22. W. Kraus, G. Nolze, Powdercell2.4, Federal 19. Institute for materials Research and Testing Rudower Chaussee 512485 Berlin, Germany.
23. T. Kokubo, H. Kushitani, S. Sakka, T. Kitsugi and T. Yamamuro, *J. Biomed. Mater. Res.*, **24**, 721 (1990).
24. RRUFF Database: Raman, X-ray, Infrared and Chemistry, RRUFF ID R070195.1
25. В. С. Горшков, В. В. Тимашев, В. Г. Савельев, Методы физико-химического анализа вяжущих веществ, Вышая школа, Москва, 1981.
26. S. R. Federman, V. C. Costa, D. C. L. Vasconcelos, V. L. Vasconcelos, *Mater. Res.*, **10**, 177 (2007).
27. M. Kimata, *N. Jb. Miner. Abh.*, **139**, 43 (1980).
28. O. M. Goudouri, E. Theodosoglou, E. Kontonasaki, J. Will, K. Chrissafis, P., Kiodis, K. M., Paraskevopoulos, A. R. Boccaccini, *Mater. Res. Bull.*, **49**, 399 (2014).

29. I. Rehman, W. Bonfield., *J. Mater. Sci.: Mater. Med.*, **8**, 1 (1997).
30. I. R. Gibson, I. Rehman, S. M. Best, W. Bonfield. *J. Mater. Sci.: Mater. Med.*, **12**, 799 (2000).
31. S. Agathopoulos, D. U. Tulyaganov, J. M. G. Ventura, S. Kannan, M. A. Karakassides, and J. M. F. Ferreira, *Biomaterilas*, **27**, 1832 (2006).
32. A. Mateus, C. Barrias, C. Ribeiro, M. P. Ferraz, F. J. Monteiro, *J. Biomed. Mater. Res.,* **86A**, 483 (2008).
33. J. Guerrero, R. Unabia, R. M. Vequizo, J. E. Gambe, M. Odarve, and B. B. Sambo, *J. Appl. Sci. Agriculture*, **9**, 321 (2014).
34. L. Radev, *Proc. Appl. Ceram.*, **8**, 155 (2014).
35. I. Fadeeva, V. Komlev, A. Gurin, A. Fomin, S. Barinov, *Powder Metallurgy Progress*, **14**, 181 (2014).
36. R. Singh, A. Srivinasan, *Ceram. Int.*, **36**, 283 (2010).
37. T. Bistey, I. Nagy, A. Simo, C. Hegedus, *J. Dent.*, **35**, 325 (2007).
38. N. Vagenas, A. Gatsouli, C. G. Kontoyannis, *Talanta*, **59**, 831 (2003).
39. M. Sato, S. Matsuda. *Zeitschrift fur Kristallographie,* **120**, 405 (1969).
40. A. Slósarczyk, Z. Paszkiewicz, A. Zima, *Ceram. Int.*, **36**, 577 (2010).
41. S. V. Dorozhkin, *J. Am. Ceram. Soc.*, **90**, 244 (2007).
42. Z. Hong, A. Liu, L. Chen, X. Chen, X. Jing, *J. Non-Cryst. Solids,* **355**, 368 (2009).
43. Y. Zhang, J. Lu, *J. Nanoparticle Res.*, **9**, 589 (2007).
44. G. S. Pappas, P. Liatsi, I. A. Kartsonakis, I. Danilidis, G. Kordas, *J. Non-Cryst. Solids*, **354**, 755 (2008).
45. L. Radev, T. Gerganov, H. Georgiev, A. Kolev, V. Vassileva, R. Iankova, E. Cholakova, *Int. J. Mater. Chem.*, **3A**, 8 (2013).
46. M. Fleet, X. Liu, *Biomaterilas*, **28**, 916 (2007).
47. M. Kharaziha, M. H. Fathi, Ceram. Int., **35**, 2449 (2009).

Table and figure captions

Table 1. Phase composition and lattice parameters for crystalline phases in the ceramics

Fig. 1. X-ray diffraction patterns of merwinite-akermanite ceramics
Fig. 2. FTIR spectra of thermally treated at 1300 ^{o}C for 2 hours ceramics
Fig. 3 SEM micrographs of the ceramic surface, after thermal treatment at 1300 ^{o}C for 2 hours
Fig 4. FTIR of the prepared ceramics, after immersion in SBF solution for 7 (a) and 14 (b) days in static conditions
Fig. 5. SEM micrographs of the ceramic surface after immersion in SBF for 7 (a, b), and 14 days (c, d)
Fig. 6 EDS data for the ceramic surface, after soaking in SBF for 7 (a) and 14 (b) days in static conditions
Fig. 7. Evolution of elemental concentrations of Ca, Mg, Si, and P in SBF solution measured by ICP-OES for different soaking times

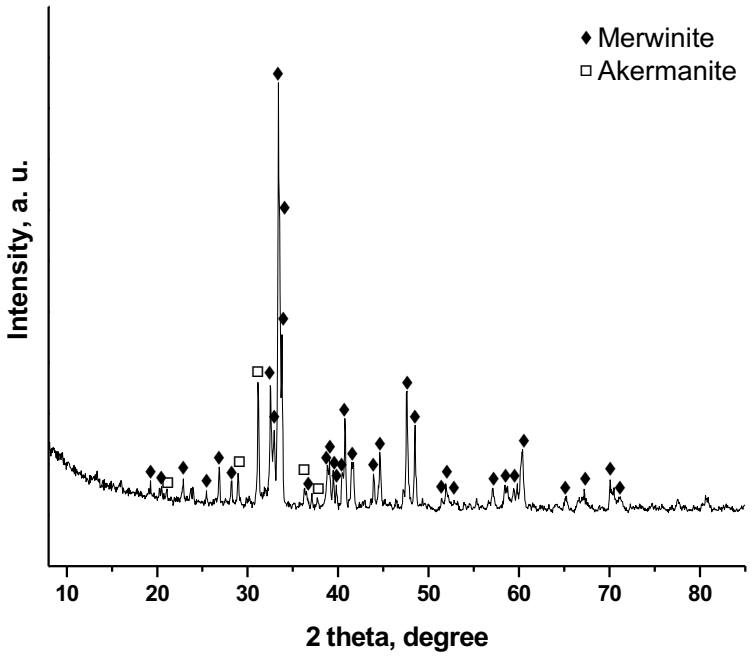

Fig. 1. X-ray diffraction patterns of merwinite-akermanite ceramics

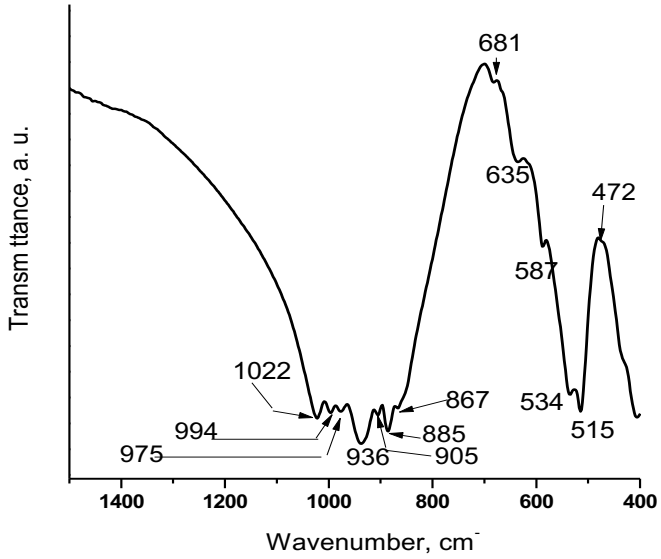

Fig. 2. FTIR spectra of thermally treated at 1200 ^{o}C for 2 hours ceramics

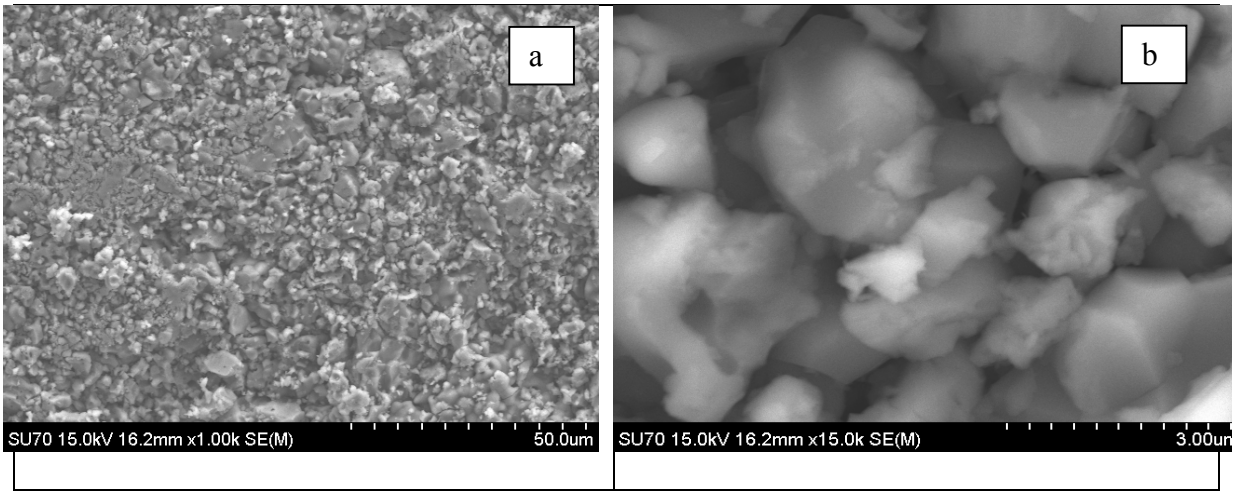

Fig. 3 SEM micrographs of the ceramic surface, after thermal treatment at 1200 ^{o}C for 2 hours

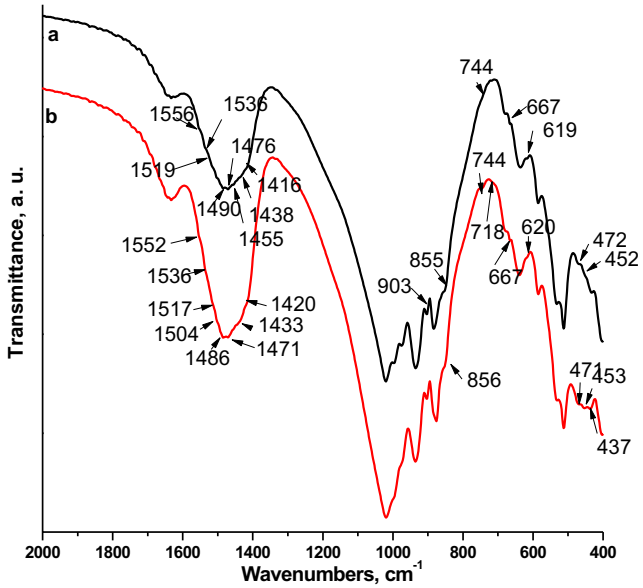

Fig 4. FTIR of the prepared ceramics, after immersion in SBF solution for 7 (a) and 14 (b) days in static conditions

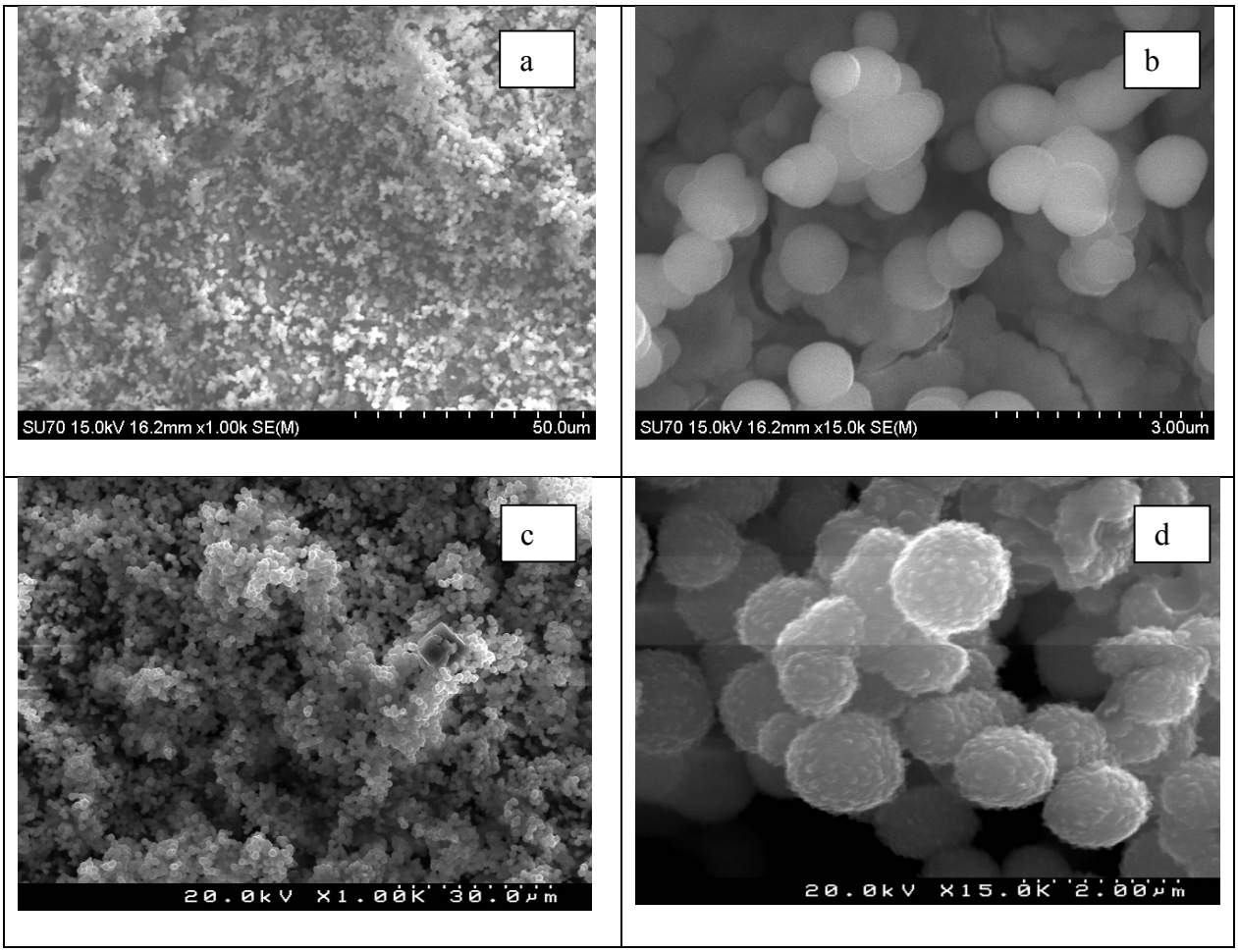

Fig. 5. SEM micrographs of the ceramic surface, after immersion in SBF for 7 (a, b), and 14 days (c, d)

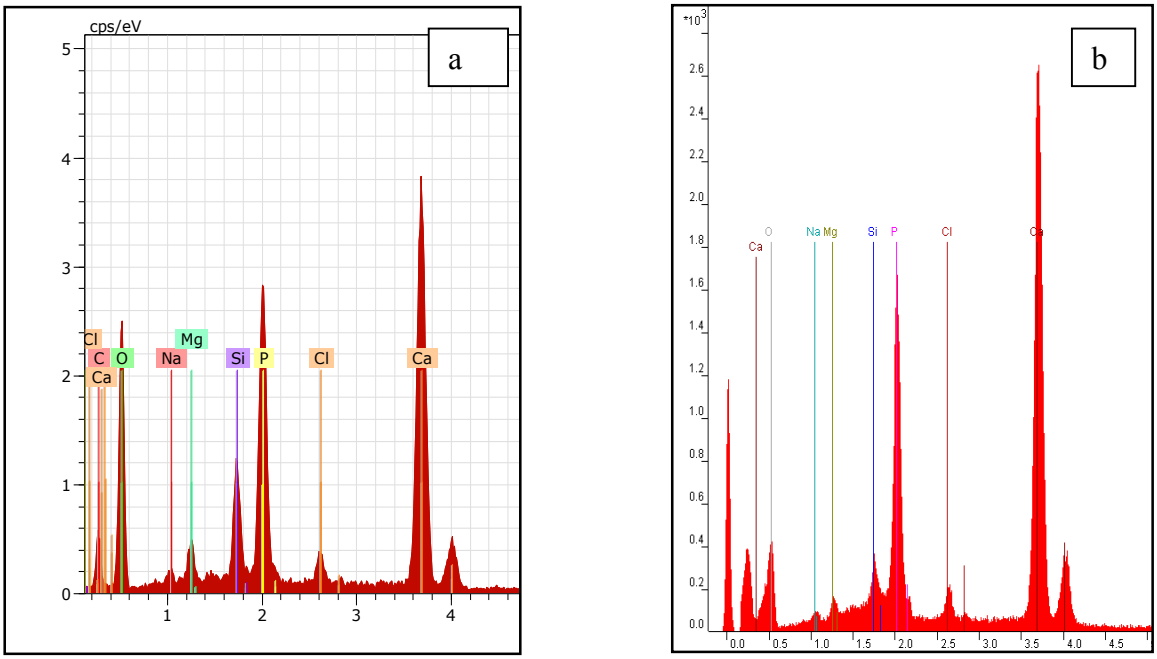

Fig. 6 EDS data for the ceramic surface, after soaking in SBF for 7 (a) and 14 (b) days in static conditions

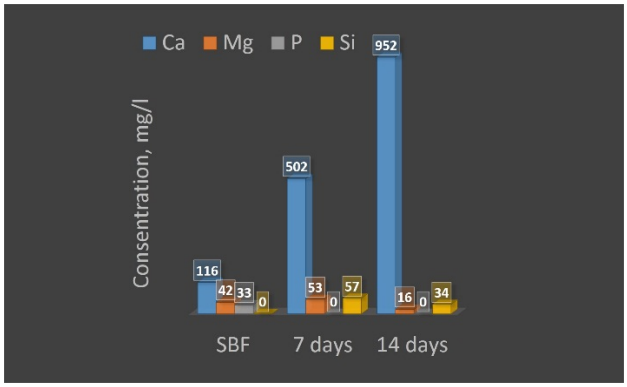

Fig. 7. Evolution of elemental concentrations of Ca, Mg, Si, and P in SBF solution measured by ICP-OES for different soaking times

Table 1. Phase composition and lattice parameters for crystalline phases in the ceramics

Crystalline phases	Concentration (vol. %)	Lattice parameters			
		a (Å)	*b* (Å)	*c* (Å)	*β* (°)
Merwinite	-	*a*	*b*	*c*	*β*
Standard JCPDS: 35-0591	-	13.29	5.304	9.352	92.09
Merwinite in ceramics	85	13.28	5.304	9.336	92.14
Akermanite	-	*a*	*b*		
Standard JCPDS: 35-0592	-	7.833	5.006		
Akermanite in ceramics	15	7.829	5.006		